KTH ROYAL INSTITUTE
OF TECHNOLOGY

Doctoral Thesis in Physics

Synthesis, Electrophoretic Deposition, and Characterization of Nanostructured Thermoelectric Materials

HAZAL BATILI

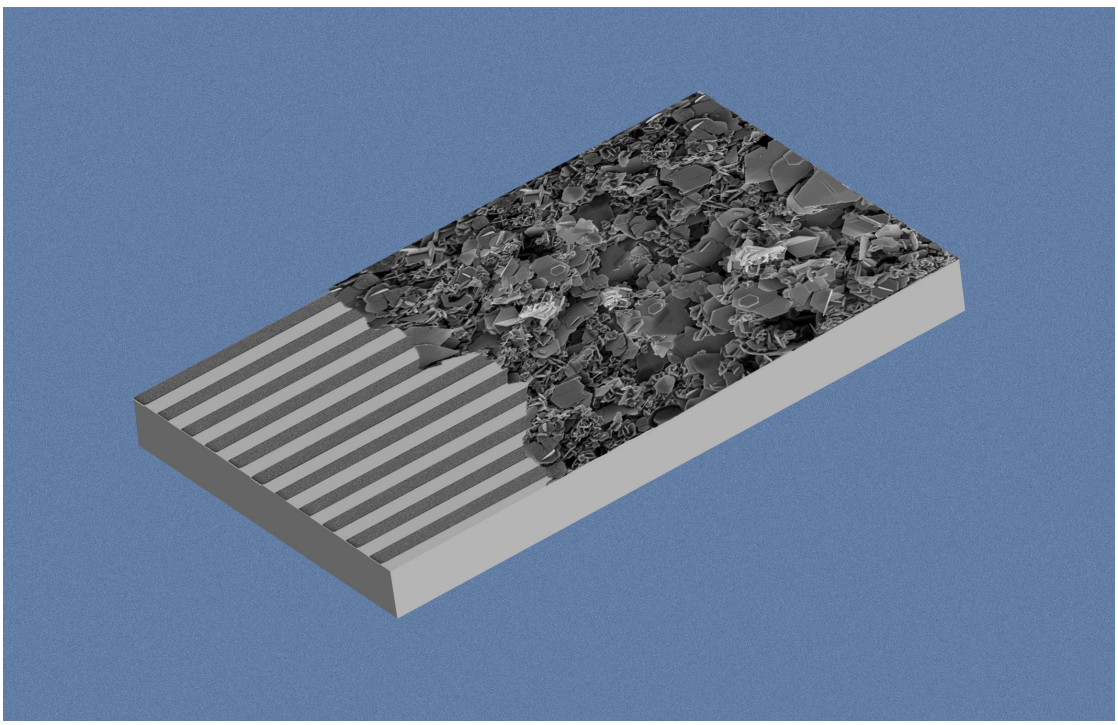

Stockholm, Sweden 2023

Synthesis, Electrophoretic Deposition, and Characterization of Nanostructured Thermoelectric Materials

HAZAL BATILI

Academic Dissertation which, with due permission of the KTH Royal Institute of Technology, is submitted for public defence for the Degree of Doctor of Philosophy on Friday the 15th September 2023, at 1:00 p.m. in FA32, Roslagstullsbacken 21, Stockholm.

Doctoral Thesis in Physics
KTH Royal Institute of Technology
Stockholm, Sweden 2023

Cover page photo: Doga Batili

TRITA-SCI-FOU 2023:38
ISBN: 978-91-8040-651-2

Printed by: Universitetsservice US-AB, Sweden 2023

Abstract

The world's increasing demand for energy and supplying this energy dominantly from fossil fuels has a major impact on global climate change. The energy crisis has gotten more alarming in the recent years which increased the motivation for replacing fossil fuels with greener routes for energy harvest. There are various technologies developed for harvesting energy, and the ability to recover energy from waste heat at a wide range of temperatures (from room temperature to more than 1000 °C) distinguished the thermoelectric (TE) materials from the rest. The drawback about the thermoelectric devices is that they are too inefficient to be cost-effective in many applications, and the developments in nanotechnology is providing some solutions to increase the efficiency of these materials and devices.

The field of thermoelectrics suffer from large discrepancy of the results in the literature, which is generally attributed to the variations in the materials qualities, urging a need for the development of synthetic techniques that can lead to large-scale TE materials in reasonable time frame. In this thesis, three different routes for rapid, scalable, and energy efficient, wet-chemical synthetic techniques for bismuth chalcogenide compounds are presented. Microwave assisted heating during reaction provided better control over the particle properties while reducing the reaction time and carbon footprint of the synthetic method, leading to materials bismuth chalcogenides with promising TE transport properties in a scalable and reproducible manner.

Hybrid TE materials, and recently emerging solid-liquid TE materials concept, requires fabrication of porous TE films, to study the effect of various interfaces, including solid and liquid electrolytes. For this purpose, we developed and optimized the electrophoretic deposition (EPD) process to prepare nanostructured porous TE films by preserving the size and morphology of the as-synthesized bismuth chalcogenide particles. A new glass-based substrate is designed and fabricated to study the electronic transport properties of the electrically active films prepared via EPD. Using this platform, we could clearly demonstrate the significance of the synthetic method on the surface chemistry and resultant transport properties of the TE materials. The methods and materials developed in this thesis are expected to impact and expedite further developments in the field of thermoelectrics.

Sammanfattning

Världens ökande efterfrågan på energi och att tillhandahålla denna energi främst från fossila bränslen har en betydande inverkan på den globala klimatförändringen. Energikrisen har blivit allt mer alarmerande de senaste åren, vilket har ökat motivationen att ersätta fossila bränslen med gröna energilösningar. Det har utvecklats olika tekniker för energiutvinning, men förmågan att återvinna energi från spillvärme vid ett brett temperaturintervall (från rumstemperatur till över 1000 °C) skiljer termoelektriska (TE) material från övriga. Nackdelen med TE-enheter är att de är för ineffektiva för att vara kostnadseffektiva i många tillämpningar, där utvecklingen inom nanoteknik erbjuder vissa lösningar för att öka effektiviteten hos dessa material och enheter.

Inom området för TE-material finns det stora avvikelser i resultaten i litteraturen, vilket i allmänhet tillskrivs variationer i materialkvaliteten. Det finns ett behov av att utveckla syntetiska tekniker som kan leda till högeffektiva TE-material i storskalig produktion på rimlig tid. I denna avhandling presenteras tre olika metoder för snabb, skalbar och energieffektiv våtkemisk syntetisering av bismutkalkogenidföreningar. Mikrovågsassisterad uppvärmning under reaktionen gav bättre kontroll över partikelegenskaperna samtidigt som reaktionstiden och koldioxidavtrycket för den syntetiska metoden minskade, vilket resulterade i bismutkalkogenider med lovande TE-transportegenskaper på ett skalbart och reproducerbart sätt.

Hybrida TE-material och det nyligen framkomna konceptet med fastvätska-TE-material kräver framställning av porösa TE-filmer för att studera effekten av olika gränssnitt, inklusive fasta och flytande elektrolyter. För detta ändamål har vi utvecklat och optimerat elektroforesdepositionsprocessen (EPD) för att framställa nanostrukturerade porösa TE-filmer genom att bevara storlek och morfologi hos de syntetiserade bismutkalkogenidpartiklarna. En ett nytt substrat baserat på glas har designats och tillverkats för att studera de elektroniska transportegenskaperna hos de elektriskt aktiva filmerna som framställts via EPD. Med denna plattform kunde vi tydligt visa betydelsen av syntesmetoden för yt-kemin och de resulterande transportegenskaperna hos TE-filmerna. De metoder och material som utvecklats i denna avhandling förväntas påverka och påskynda vidareutvecklingen inom forskningsområdet för TE-material.

List of papers

Paper A

B. Hamawandi, S. Ballikaya, **H. Batili**, V. Roosmark, M. Orlovská, A. Yusuf, M. Johnsson, R. Szukiewicz, M. Kuchowicz, and M. S. Toprak, Facile solution synthesis, processing and characterization of n- and p-type binary and ternary Bi-Sb tellurides, *Applied Sciences* **10**, 1178 (2020).

Paper B

B. Hamawandi, **H. Batili**, M. Paul, S. Ballikaya, N. I. Kilic, R. Szukiewicz, M. Kuchowicz, M. Johnsson, and M. S. Toprak, Minute-made, high-efficiency nanostructured Bi_2Te_3 via high-throughput green solution chemical synthesis, *Nanomaterials* **11**, 2053 (2021).

Paper C

H. Batili, B. Hamawandi, A. B. Ergül, and M. S. Toprak, On the electrophoretic deposition of Bi_2Te_3 nanoparticles through electrolyte optimization and substrate design, *Colloids and Surfaces A: Physicochemical and Engineering Aspects* **649**, 129537 (2022).

Paper D

H. Batili, B. Hamawandi, P. Parsa, A. B. Ergül, R. Szukiewicz, M. Kuchowicz, and M. S. Toprak, Electrophoretic assembly and electronic transport properties of rapidly synthesized Sb_2Te_3 nanoparticles, *Applied Surface Science* **637**, 157930 (2023).

Paper E

H. Batili, B. Hamawandi, A. B. Ergül, R. Szukiewicz, M. Kuchowicz, and M. S. Toprak, Electrophoretic deposition and characterization of Bi_2Te_3 synthesized through hydrothermal and thermolysis routes, *Colloids and Surfaces A: Physicochemical and Engineering Aspects* **Under Review**.

Other publications

The author has contributed to the following publications, which are not related to the subject of this Thesis.

Z. Lalegani, S. S. Ebrahimi, B. Hamawandi, L. Spada, **H. Batili**, and M. S. Toprak, Targeted dielectric coating of silver nanoparticles with silica to manipulate optical properties for metasurface applications, *Materials Chemistry and Physics* **287**, 126250 (2022).

B. Hammarström, T. J. Lane, **H. Batili**, R. Sierra, M. Wiklund, and J. A. Sellberg, Acoustic focusing of protein crystals for in-line monitoring and up-concentration during serial crystallography, *Analytical Chemistry* **94**, 12645 (2022).

Author's Contribution

Paper A: Facile solution synthesis, processing and characterization of n- and p-type binary and ternary Bi-Sb tellurides

The author contributed to the physicochemical characterization of the particles specifically to the study of colloidal stability of all the compounds. Author was also involved in the writing and editing of the paper.

Paper B: Minute-made, high-efficiency nanostructured Bi_2Te_3 via high-throughput green solution chemical synthesis

The author contributed to the physicochemical characterization of the particles specifically to the study of colloidal stability of all the compounds. Author was also involved in the writing and editing of the paper.

Paper C: On the electrophoretic deposition of Bi_2Te_3 nanoparticles through electrolyte optimization and substrate design

The author was the main responsible of the paper, assisting the particle synthesis, preparing the thermoelectric films via electrophoretic deposition (EPD), optimizing the EPD parameters, fabricating electrodes via photolithography, microstructure analysis of the films, data analysis, writing and editing the paper.

Paper D: Electrophoretic Assembly and Electronic Transport Properties of Rapidly Synthesised Sb_2Te_3 Nanoparticles

The author was the main responsible of the paper, assisting the particle synthesis, preparing the thermoelectric films via electrophoretic deposition (EPD), fabricating electrodes via photolithography, microstructure analysis of the films, data analysis, writing and editing the paper.

Paper E: Electrophoretic deposition and characterization of Bi_2Te_3 synthesized through hydrothermal and thermolysis routes

The author was the main responsible of the paper, assisting the particle synthesis, preparing the thermoelectric films via electrophoretic deposition (EPD), fabricating electrodes via photolithography, microstructure analysis of the films, data analysis, writing and editing the paper.

Contents

Chapter 1

Introduction

1.1 Thermoelectric (TE) materials

The energy crisis in the world have become increasingly severe and urgent, which is forcing many countries to leave the usage of fossil fuels behind and to adopt greener routes to overcome this crisis. There are multiple technologies that can provide greener solutions for energy generation and storage, including photovoltaics, wind and water turbines, batteries, and thermoelectric (TE) converters [1–5]. The process of energy conversion from a primary energy source to the end use is subjected to several losses at almost every step of the conversion [6]. Forman et al. reported that 72% of the global primary energy consumption is lost after conversion, and 63% of the waste heat arises below 100 °C where the largest portion comes from electricity generation [6]. To increase the energy efficiency and reduce the energy consumption, it is essential to use such waste heat. TE materials can convert the waste heat into electricity: when there is a temperature difference across the TE material, the charge carriers diffuse away from the hot side and accumulate on the cold side. The flow of charge carriers creates a voltage difference which is directly proportional to the temperature difference across the material, and this phenomenon is called the Seebeck effect. The reverse, i.e. the Peltier effect, is also possible, application of electrical current to a TE material causes the diffusion of charge carriers from hot side to the cold, creating a temperature difference, which can be used as heating or cooling element. Thermoelectric generators (TEGs) are solid state semiconductor devices containing many thermocouples (TCs) that are connected electrically in series and thermally in parallel. Every TC in a TE device consists of one n- and one p-type semiconductor, in which the charge carriers are electrons and holes, respectively. These n- and p-type couples are connected to each other with metallic contacts (Figure 1.1).

To evaluate the performances of TE materials, a dimensionless quantity has been formulated which is referred to the TE figure of merit (ZT). This value can be calculated via $ZT = (S^2 \sigma T)/\kappa$, where S, σ, κ and T are the Seebeck coefficient, electrical conductivity, total thermal conductivity, and the absolute temperature (Kelvin), respectively. The total thermal conductivity is the sum of electrical and lattice thermal conductivity, $\kappa = \kappa_e + \kappa_l$. An ideal TE material should have high Seebeck coefficient and low thermal conductivity. However, these two transport properties have a strong connection with each other, and it is crucial to find effective ways to break this correlation to improve the performances of TEGs.

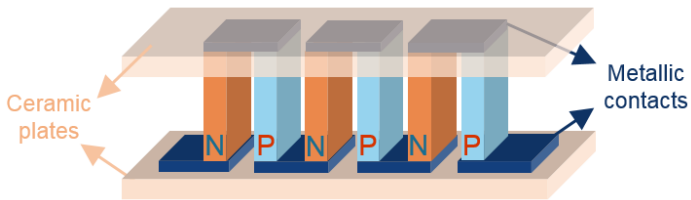

Figure 1.1. A typical design of TEGs where many n- and p-type semiconductors are connected electrically in series via metallic contacts to obtain the desired electric current and voltage. The thermocouples are generally placed between two ceramic plates.

This thesis work focuses on inorganic crystalline TE materials, more specifically $Bi_{2-x}Sb_xTe_3$ (x:0-2) compounds, where the atoms are regularly arranged in the form of lattice inside the crystals. The carriers of electric charge and thermal energy move in these crystal lattices, thus it is important to understand the crystal structure of the materials to be able to tune their electrical and thermal conductivity. Bi_2Te_3 and Sb_2Te_3 compounds have been dominating the research for near room temperature thermoelectric applications with their outstanding ZT values [7–9]. Both compounds have a rhombohedral crystal structure, and in each atomic layer, atoms are stacked in a hexagonal pattern [10–12]. The hexagonal unit cell consists of five covalently bonded monatomic sheets of Bi-Te or Sb-Te along the c-axis in the sequence of -Te(1)-Bi/Sb-Te(2)-Bi/Sb-Te(1)-Te(1)-Bi/Sb-Te(2)-Bi/Sb-Te(1)-, and a weak van der Waals attraction between the layers of -Te(1)-Te(1)- where (1) and (2) represents the two different chemical states of Te atoms [10, 12]. Having these large and highly polarizable Te atoms with relatively weak bonds is the intrinsic reason for the low κ_l of these compounds [9, 11]. Defects and doping these crystals are important to improve the TE performance of the materials, for instance, optimization of carrier concentration is necessary to have a peak in ZT at desired temperatures (Figure 1.2) [9].

1.1.1 Nanostructured TE materials

Nanostructured TE materials have been studied widely to overcome the bottleneck about the correlation between parameters determining the ZT [13–15]. Several strategies have been tested to reduce the κ and/or increase the S and σ, such as band gap engineering by tuning the doping and composition, and by investigating the effects of grain boundaries, and porosity [8, 16–18]. However, the correlation between S, σ, and κ_e through carrier concentration and effective mass makes it difficult to tune these properties [19]. For this reason, research on enhancement of TE performance mainly focuses on the decrease of κ_l as it is being the more independent parameter.

The electronic component of the total thermal conductivity, κ_e, can be defined as the heat transport of charge carriers among the crystal, and it can be calculated via Wiedemann-Franz law: $\kappa_e = L\sigma T$ where L is the Lorenz number, σ is the electrical conductivity and T is the absolute temperature. To achieve high ZT values, low κ_e and high σ values are needed, but the Wiedemann-Franz law shows the dependence of these values on each other [8]. However, the second component of κ, κ_l, is a result of phonons travelling through the crystal lattice, which is regulated by the size and porosity of the crystal grains [13,18]. It can be tuned with nanostructuring of TE materials, by choosing the length scale of these structures based on the difference between mean free path of electrons and phonons, phonon scattering can be increased instead of electrons, which would reduce the κ_l [13, 18]. When grain size is comparable to phonon mean free path, grain boundary scattering increases and the phonon transport would be blocked. Tailoring the crystal grain size to reduce κ_l is a well known technique to obtain high performance TE materials [13, 18].

1.2 Synthesis of TE materials

Nanostructured tellurium (Te)-based compounds such as, Bi_2Te_3 and Sb_2Te_3, has been studied widely over the past decades due to their high ZT values near room temperature [7, 16]. There are various synthesis techniques to prepare these type of materials; mechanochemical [20, 21], hydrothermal [22, 23], solvothermal [13, 24], and microwave (MW) assisted routes [25, 26].

A typical synthesis of TE particles via mechanochemical method consists of ball milling for around 10-20 h, followed by hours of drying and sintering of the powder, which is not time or energy efficient way to prepare these materials [20, 21, 27]. Since it is difficult to control the particle size and morphology by using this type of top-down physical techniques,

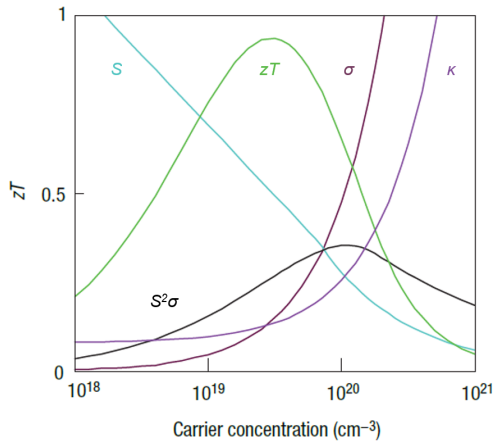

Figure 1.2. Optimization of ZT by tuning the carrier concentration. Good TE materials are typically heavily doped semiconductors, and improving their efficiency (ZT) involves a compromise of κ, S, and σ. Materials with low carrier concentration (insulators and some semiconductors) have large S, but low κ and σ, which is not beneficial for TE materials. The peak of ZT typically occurs at carrier concentrations between 10^{19} to 10^{20} carriers per cm^3, (as in some metals and semiconductors) where the material has relatively high S and σ, and low κ [8].

bottom-up chemical routes, such as solvothermal and hydrothermal, are more commonly preferred for the preparation of nanostructured TE materials. Also, the possibility of scaling up the synthesis makes the chemical routes more attractive. However, when the synthesis is performed in an autoclave, the reaction time differs from 4 to 48 hours, normally for lower temperatures (around 150-180 °C) reaction time is longer (24-48 h) [13, 22–24]. Using a MW reactor in solvothermal or hydrothermal synthesis, decreases the reaction time into minutes, which is more sustainable and environmentally friendly [25, 26]. Additionally, the rapid and homogeneous heating facilitates the control of particle shapes and sizes. This economically viable heating method makes it possible to do large scale synthesis of bulk nanomaterials.

In this thesis work, three different MW-assisted synthetic routes were used for the preparation of TE materials. In Paper A, polyol method for the preparation of binary and ternary $Bi_{2-x}Sb_xTe_3$ compounds, and in Paper B, a comparison of hydrothermal and polyol routes for synthesis of Bi_2Te_3 has been reported. The synthesis of Sb_2Te_3, and Bi_2Te_3 particles via thermolysis route is presented in Paper D, and Paper E, respectively. Further details of the syntheses will be discussed in Chapter 2.

1.3 Processing of TE materials

The bismuth antimony telluride (BiSbTe) bulk alloys are generally densified from ball-milled powders via pre-pressing into pellets (cold pressing), or using hot densification with pressure (hot pressing or spark plasma sintering) or without pressure (pressureless sintering) [16, 28–31]. In hot pressing process, temperature and pressure are applied simultaneously to the powder compact contained in a die, and in cold pressing there is no heating but only pressure is applied. Pressureless sintering is also commonly used where the powder is poured into a metal die and vibrated until it is loosely compacted, then the die is placed into a furnace and the material is sintered. The spark plasma sintering (SPS) is different from the other methods since in this process a simultaneous application of pressure and pulsed direct current is used to press the powder inside the die, between two conducting punches. In Paper A and B, as-synthesized TE nanopowders were consolidated via SPS method to obtain nanostructured bulk solid materials in pellet form, and after SPS, the pellets were sintered and polished for further analysis.

In low dimensional materials, it is easier to control the material properties, such as composition and microstructure, that have high impact on the TE properties. There are various techniques to prepare TE films such as drop casting [24], sputtering [32], thermal evaporation [33], Dr. blading [34], and electrophoretic deposition (EPD) [35, 36]. When compared to other techniques EPD is relatively cost effective since it does not require expensive equipment and infrastructure. It is a time-efficient process where one can prepare films within minutes with many different materials and material combinations such as biomaterials [37], polymers and proteins [38], graphene-based materials [39], metal oxides [40], photocatalytic materials [41], and semiconductors [35]. Also, EPD has the potential to scale up the deposition area from microns to meters, and providing the possibility to do film preparation on different geometries. The crystallinity and composition of the deposited material is the same with bulk since there are no chemical reactions occurring during EPD process. In Paper C, D and E, the EPD technique is used to prepare TE films.

1.3.1 Spark Plasma Sintering (SPS)

Spark plasma sintering (SPS) is an unconventional sintering technique that uses pulsed electric current to obtain nanostructured bulk solid materials. The usage of current instead of conventional heating provides shorter sintering times and lower temperatures, which minimizes the post-synthetic crystal grain growth of nanoparticles [30, 31]. In conventional hot pressing, the temperature and pressure is applied to the whole die containing

the powder, hence, the heating of the sample is slow and not homogeneous, which is causing an increase in grain size and decrease in number of grain boundaries. Applying direct current and pressure to the conducting die facilitates the sintering process, providing more homogeneous heating along the sample, which minimizes the grain growth and increases the number of grain boundaries that is essential for phonon scattering. Increasing the phonon scattering at the grain boundaries is an effective method to reduce the thermal conductivity of TE materials and increase their ZT values.

1.3.2 Electrophoretic Deposition (EPD)

The migration and separation of ions in a solution under the influence of an applied electric field is defined as electrophoresis. Electrophoretic deposition (EPD) is a method that uses electrophoresis to migrate and deposit charged particles on to the surface of the oppositely charged electrode. In an EPD setup, there are two electrodes partially placed in a conducting media containing the target particles, in which an electric field is applied from a power source through the electrodes Figure 1.3. The deposition can be made directly onto the electrode or on a conductor/semiconductor substrate that is attached to it, this electrode where the film is forming, can be referred to as the working electrode (WE). The second electrode is the counter electrode (CE) which is used to create the electric field. The particle deposition can be on either the positive or the negative electrode, which is determined by the surface charge of the particles in the EPD media. The details of the EPD process is presented in Chapter 3.

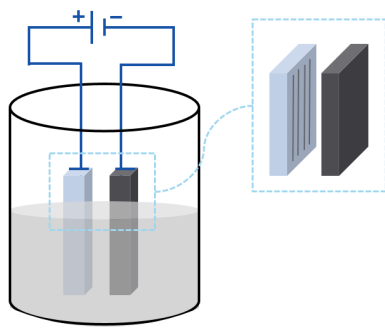

Figure 1.3. A schematic showing an EPD setup, black lines representing a container in which an electrolyte is placed (shown in light gray). There are two electrodes partially dipped in the electrolyte, blue one represents the glass-based working electrode and dark gray is the stainless steel counter electrode, both of them are connected to a power supply.

1.4 Objectives

Thermoelectric devices have a vital role in waste heat recovery, but their performances still need improvement, which can be achieved by using nanostructured TE materials. The aim of this thesis work was to develop a platform, which can be used to prepare nanostructured porous TE films, where the effects of different molecular linkers, particle sizes and morphologies, on the TE performance of the material can be investigated. We develop fast, scalable and energy efficient methods to synthesize n- and p-type $Bi_{2-x}Sb_xTe_3$ compounds with desired size, morphology and surface chemistry. Also, study the effects of the solvents and precursors used in the synthesis on the surface chemistry and TE properties of the particles. The implementation and optimization of electrophoretic deposition process for the preparation of porous nanostructured TE films, controls the quality and quantity of the deposited films. We test organic molecular linkers in porous TE films in order to improve the power factor.

Chapter 2

Synthesis and material characterization

Three different MW-assisted chemical routes have been established for the synthesis of TE materials, in each section of this chapter an introduction of the synthesis method and a summary of the results are presented.

2.1 Polyol synthesis (Paper A)

In organic chemistry, polyol is defined as an alcohol with multiple hydroxyl groups. Chemically, the most basic polyol compound is ethylene glycol (EG) which contains two -OH groups. In these types of molecules as the number -OH groups increase, the boiling point, viscosity, and polarity of the compound increases [42]. Polyols are considered water-equivalent molecules with high boiling points, since their solubility is very similar to water. Polarity of water is higher than the polyols but their lower polarity is compensated by their superior chelating properties. Chelating molecules have the ability to bind the metal ions, which is a beneficial material property for controlling nucleation, particle growth and agglomeration, as polyols can adhere on particle surfaces and act as colloidal stabilizers [42]. Their high boiling points are also critical for the colloidal stabilisation, as they allow high reaction temperatures (200-320 °C) without the need of an autoclave or application of high pressure [42]. Liquid phase synthesis of crystalline nanomaterials often requires high temperatures to avoid post-sintering of the powders, since it can cause an uncontrolled crystal growth and agglomeration. All these advantages of the polyol method enabled the preparation of high purity nanostructured binary and ternary metal chalcogenides, the details of synthesis and material characterization is presented in Paper A.

$Bi_{2-x}Sb_xTe_3$ compounds were prepared by tuning the material composition directly in EG solution without any requirement of post-processing. Rapid and homogeneous heating of the MW reactor resulted in very short reaction time (2 min) and high yield (>8 g per batch). Another advantage of the MW heating was the controlled growth of $Bi_{2-x}Sb_xTe_3$ (x:0-2) nanoplatelets with high crystallinity and phase purity that were characterized with x-ray powder diffraction (XRPD). Crystal phases were analyzed for both as-synthesized powders and sintered pellets. A rhombohedral crystal structure with no impurities were observed in two n-type (Bi_2Te_3 and $Bi_{1.8}Sb_{0.2}Te_3$) and two p-type (Sb_2Te_3 and $Bi_{0.5}Sb_{1.5}Te_3$) compositions. Scanning electron microscopy (SEM) analyses showed hexagonal platelet morphology for all the different composition of particles, which was in agreement with their rhombohedral crystal structures.

X-ray photoelectron spectroscopy (XPS) was used to study the surface chemistry of the as-synthesized powders, where carbon residue and three different metallic and oxide phases were identified; TeO_2, Bi_2O_3, and Sb_2O_3. The Bi_2Te_3 and Sb_2Te_3 samples had similar content of TeO_2, while the other oxide phases (Bi_2O_3 and Sb_2O_3) changed in quantity depending on the x value. The oxide content of the particle surface has an influence on the surface charge, which can be measured with zeta potential analysis. Formation of a net charge on the particle's surface affects the ion distribution at the interfacial area, which leads to a higher concentration of counterions near the surface. When the surface charge is balanced by the thin layer of counter ions at the surface, then the net charge becomes zero, this point is called isoelectric point (IEP). The zeta potential of the particles were measured as a function of pH, and the IEP was determined for each composition. The synthesis method and surface stabilizers used in the reaction determine the surface chemistry of the particles. The study of changes in surface charge as a function of pH is an important indication of colloidal stability of the materials.

2.2 Hydrothermal synthesis (Paper B, C and E)

Solvothermal and hydrothermal syntheses has been used for many decades as a solution-based chemical route for material synthesis [43]. Typically the syntheses are conducted either in a sealed container, or in a high-pressure autoclave under the solvent's subcritical or supercritical conditions [43]. In the hydrothermal route, the chemical reaction takes place in an aqueous solution above the boiling point of water. The selection of the synthetic route, and solvents used in the reaction determine the crystallinity and phase purity of the particles [14,44]. In Paper A and B, EG is used as a solvent in MW-assisted polyol synthesis, which is an abundant, non-volatile, and low tox-

icity compound with low dielectric constant (37 at room temperature). In hydrothermal route the solvent is water, which is the most environmentally friendly material with high dielectric constant (78.5 at room temperature). MW heating is based on the direct electromagnetic energy absorption of the solvent and the conversion of this electromagnetic energy into heat [45]. This capability of energy conversion depends on the dielectric properties of the material. MW-assisted synthesis reduces the reaction time by increasing the overall reaction kinetics as a result of localized heating [46]. The superheating of the solvent can cause changes in its dielectric constant, for instance, the dielectric constant of water decreases with increasing temperature, around 200 °C it reduces to 30 [47, 48]. Lower dielectric values reveal a better capacity to absorb microwave energy, resulting in an efficient way of heating the sample [45]. Therefore, the combination of MW-assisted heating and hydrothermal synthesis enables the development of a fast and effective way of nanocrystal growth.

Bi_2Te_3 nanoparticles (NPs) were synthesized via MW-assisted hydrothermal and polyol methods, material properties of the end products were compared and discussed in Paper B. Both syntheses were conducted at 220 °C in 2 min and after cooling down, particles were washed and dried. Using XRPD for the structural analysis of the as-made powders, and pellets prepared via SPS, it has been found that from both syntheses, particles with rhombohedral crystal structure were obtained. For the surface analysis, XPS measurements were performed on as-synthesized particles, and the results showed that due to the different precursor and structure directing agents used in the synthetic methods, Bi and C speciation was different on the particles' surfaces. In polyol route, Bi precursor prepared by dissolving $BiCl_3$ in EG (solvent and reducing agent) then thioglycolic acid ($C_2H_4O_2S$, TGA) was added to the mixture, and for Te precursor, Te powder was mixed with trioctylphosphine ($C_{24}H_{51}P$, TOP). Carbon content in this sample was dominantly indexed to C-O bonds that can be attributed to the conjugation of TGA to the NP surface through sulfur atoms. In case of bismuth content, elemental Bi was only found in oxide state in polyol sample, but the Te content was similar in both samples that were in both metallic and oxide states. In hydrothermal route precursors ($BiCl_3$ and Na_2TeO_3), shape directing agent (ethylenediaminetetraacetic acid-$C_{10}H_{16}N_2O_8$, EDTA) and reducing agent, (sodiumborohydride-$NaBH_4$) are mixed in one pot where water was the solvent. The carbon speciation of the sample was mainly indexed to C-O/C-N content, which can be a result of using EDTA as the surface directing agent, as it is known to be a hexadentate ligand at pH above 10. The Bi content of the sample consisted of both oxide and metallic states, where the oxide had higher fraction than the metallic state.

2.3 Thermal decomposition (thermolysis) (Paper D and E)

Thermal decomposition (thermolysis) is a synthesis method which can be used for nanoparticle synthesis by dissolving metal-organic compounds as precursor in high boiling point organic solvents, such as oleylamine ($C_{18}H_{37}N$), oleic acid ($C_{18}H_{34}O_2$, OA), and 1-octadecene ($C_{18}H_{36}$, ODE) [49–52]. Long alkyl chain groups in the metal-organic compound are used as passivating ligands by covering the surface of the crystal to prevent agglomeration [49, 51]. Unlike solvothermal method, in thermolysis typically reaction temperature does not exceed the boiling point of the organic solvent.

In Paper D, we presented the synthesis of Sb_2Te_3 NPs via thermolysis, the precursors were $SbCl_3$ and Te powder, combination of organics used as solvents (OA, ODE and tributylphosphine-$C_{12}H_{27}P$, TBP), and TGA was the shape directing agent. Reaction was conducted at 220 °C in 2 min in MW-oven. After cooling down, particles were washed and dried at 60 °C under vacuum. For the structural analysis of as-synthesized particles XRPD measurements were done, where the diffraction pattern showed a crystalline phase indexed to Sb_2Te_3 rhombohedral crystal structure with no observation of additional peaks, indicating high purity of the material.

Surface chemistry of the as-made particles identified two different Te phases, where the metallic phase had slightly higher fraction than the oxide phase. For Sb content, again two phases were identified, metallic and oxide, but Sb_2O_3 had much lower fraction than the metallic phase. Microstructure analysis was done with SEM, showing hexagonal platelet morphology and intergrown particles. The successful control of the particle morphology is achieved via the use of TGA as shape directing agent, which passivates the lateral faces of the hexagonal platelets and leads the growth sideways. In Paper E, Bi_2Te_3 NPs prepared via thermal decomposition method was used to prepare TE films. The synthesis was very similar to Sb_2Te_3, where the Sb precursor is replaced with Bi precursor $BiCl_3$. The rest of the procedure followed was kept identical to Sb_2Te_3 synthesis. XRPD analysis of the as-made particles showed high purity crystalline phases indexed to Bi_2Te_3 with rhombohedral crystal structure.

Chapter 3

Electrophoretic deposition of TE materials

3.1 EPD set-up and substrates

In EPD experiments a Voltcraft CPPS-160-84 power supplier was used in constant-voltage mode. Two electrodes, i.e. counter (CE) and working (WE) electrode, were connected to the power supplier with alligator clips, they were kept parallel to each other with a separation distance of 1.5 cm (Figure 1.3). A glass beaker placed on a lab jack (stage) was used to contain the EPD media (electrolyte). The bottom edges of the electrodes were kept ~ 1 mm above the bottom of the glass beaker. Stainless steel sheets were used as counter electrode. For working electrode two different designs were tested, first one was a stainless steel electrode with a substrate (Si wafer) attached to it using a Cu tape (Figure 3.1). The Si wafer being a semiconductor, it was interrupting the transport property measurements of the deposited TE films. To prevent this interruption we designed a glass-based electrode which was fabricated via maskless photolithography.

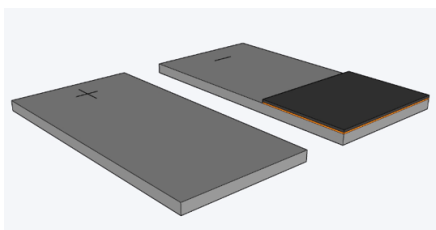

Figure 3.1. Stainless steel electrodes; CE (+), and Si wafer shown in black was attached to the WE (-) with a Cu tape.

3.1.1 Glass-based substrate preparation

The transport property measurements of the deposited films are very critical for the evaluation of the TE performances of the films. To be able to perform uninterrupted and reliable measurements an insulating substrate was necessary, therefore, a glass-based electrode/substrate was designed and fabricated via maskless photolithography. Soda lime photo mask blanks (3x3x0.06 inch) coated with low reflective chrome and 0.53 μm thick AZ 1500 positive photoresist layers were used. To transfer the pattern that is designed in KLayout software, Advanced Maskless Aligner (MLA 150, Heidelberg Instruments) was used with an exposure dose of 140 mJ/cm^2. Exposure time was 30 min per mask blank when 10 μm wide lines were used (Figure 3.2). Maskless photolithography was time- and energy-efficient way to fabricate these microstructures, since there was no need for mask preparation. When the positive photoresist was exposed to UV light with a focused laser beam (λ = 375 nm), the chemical structure of the resist changes and becomes more soluble in the photoresist developer (Microposit Developer MF 309) (Figure 3.3). Following the exposure, substrates were developed for 1 min to remove the part of the resist that was exposed to UV light, then etched for 40 s in chromium etchant to create the Cr pattern and transferred into AZ 100 remover bath to clean all the remaining photoresist (Figure 3.3). Between these steps sample was washed with MilliQ water and dried with an air gun. Prior to EPD experiments glass-based electrodes were cut into pieces with desired dimensions using a diamond pen, and washed with acetone and distilled water.

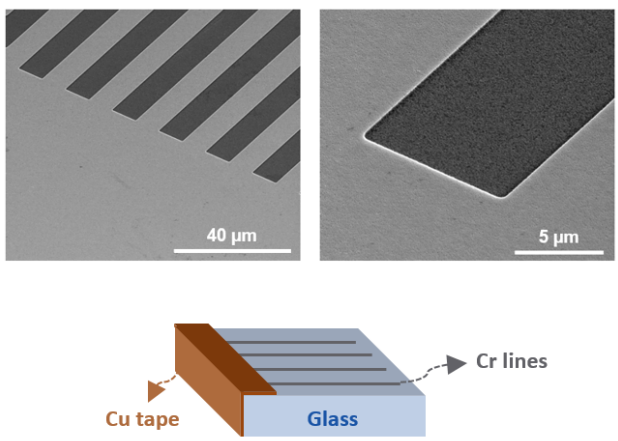

Figure 3.2. SEM images of Cr lines on glass, line width and separation is 10 μm.

Different line width and line separations were tested for the pattern design; 1, 2, 5, and 10 μm wide Cr lines were exposed on the glass (Figure 3.4). The aim of this test was to observe if it is possible to deposit particles continuously throughout the electrode, or whether the deposition will be only on Cr lines and not on the glass. In all four different line widths, there were homogeneous particle deposition. The 10 μm wide lines were chosen for the electrode design to be used in future experiments, since thinner lines were more time consuming to fabricate via photolithography (Figure 3.2).

In EPD process, an electric field is necessary to migrate the charged particles in the solution, hence, both electrodes has to be conducting. The Cr lines fabricated on the glass electrode are not connected to each other, which makes the electrode an insulator (Figure 3.2). To connect the lines a Cu tape was attached at one end of the lines. An alligator clip, connected to the power source, was placed on the Cu tape during EPD process. When the deposition was completed, the tape was removed to disconnect the lines, so that, the conductivity of the substrate does not interrupt the transport property measurements. The results of the transport measurements will be discussed in Chapter 4.

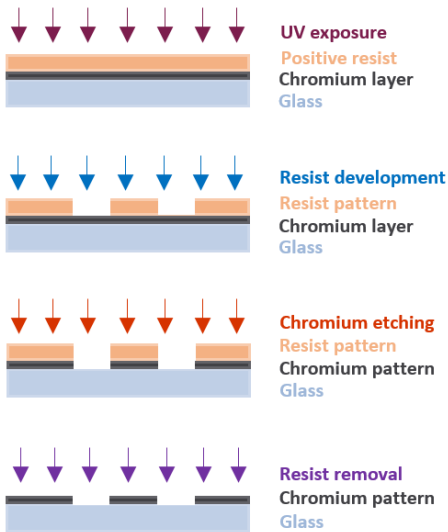

Figure 3.3. Glass electrode preparation steps via maskless photolithography; first step is direct writing of the pattern on to substrate, then resist development to remove parts of photoresist that was exposed to UV light. Next step is etching through the Cr layer, and the last step is resist removal leaving a glass substrate with Cr pattern on it.

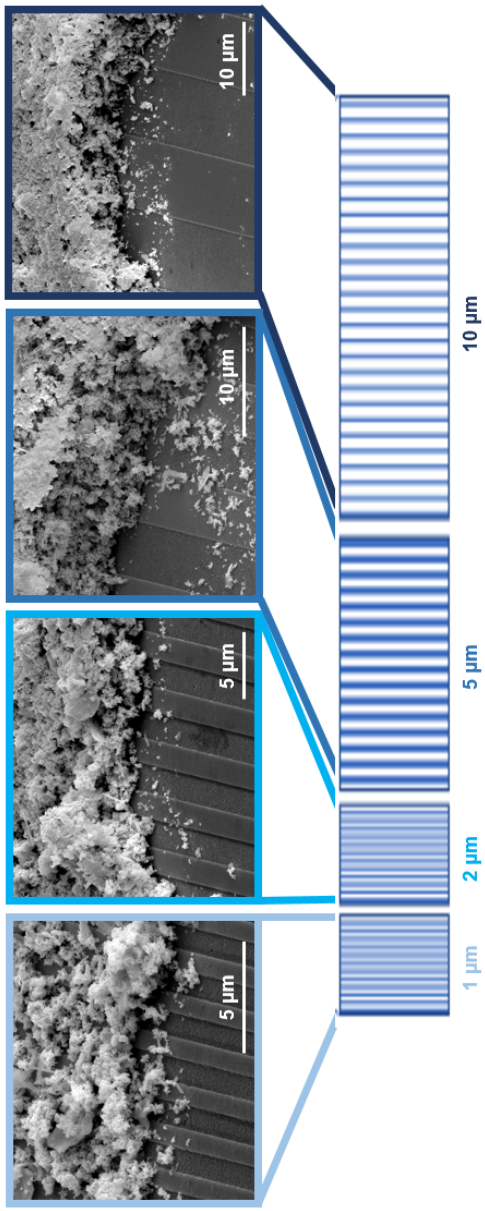

Figure 3.4. SEM images of the deposited particles on glass substrates with various line width and separation; from bottom to top, line width increases from 1 to 10 µm.

3.2 Optimization of EPD parameters

The quality of the films and the quantity of the deposited material depend on many parameters, which can be divided into two groups; those related to the EPD setup and those to the colloidal dispersion. Applied voltage, inter-electrode distance, and deposition time are the parameters related to the setup. Particle size, zeta potential and properties of the liquid media (viscosity, dielectric constant, conductivity) are the parameters related to the suspension. Strength of the applied electric field directly affects the deposition yield. Application of higher potential shortens the deposition time and increases the yield [53]. However, this doesn't indicate that stronger electric field improves the quality of the deposited film. It has been reported that using moderate fields (25-100 V/cm) creates more uniform films whereas using stronger fields lowers the film quality [54]. Particle deposition on the electrode surface is a kinetic phenomenon, since the packing density of particles is affected by their accumulation rate [53]. The application of high electric field can cause a turbulence in the electrolyte, the flow of surrounding liquid medium can disturb the coating by affecting the particle movement [53]. Under constant voltage and particle concentration, when the EPD duration increases, at the beginning and the deposition rate increases after a while reaches a plateau [53–55]. As the particles begin to deposit on the electrode surface, an insulating layer starts to form and in time the thickness of the deposited film increases, which deteriorates the electric field preventing particle migration toward the oppositely charged electrode.

The effects of applied electric field and deposition time have been studied in Paper C. By increasing the applied voltage from 70 to 80 V while keeping deposition time and distance between electrodes constant, an increase in film thickness was observed due to the increase in the amount of particles deposited on the electrode surface, i.e. deposition yield increased with stronger electric field. To test the deposition time, the electric field strength was kept constant while time increased from 3 to 4 min, and an increase in deposited film thickness was observed since there wasn't enough deposited particles to form an insulating layer at the electrode surface. A smooth and uniform Bi_2Te_3 film is prepared with higher electric field strength and lower deposition time (Figure 3.5).

The second group of parameters define the stability of the colloidal system. The main factors are particle size and surface properties, interparticle interactions, and the interaction between particles and liquid media [56]. There is a well-defined separation between dispersed particles and the surrounding medium, and this interface determines the surface properties, such as adsorption, surface charge and electrical double layer [56]. During

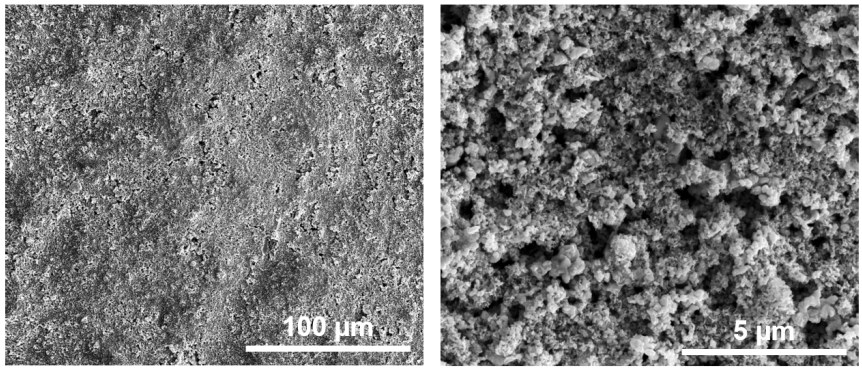

Figure 3.5. SEM micrographs of Bi_2Te_3 at different magnifications, the film was deposited at 80 V and 3 min.

the EPD process, to be able to prepare a homogeneous and smooth film, it is essential that particles remain dispersed and stable in the solution [53]. Larger particles tend to settle down due to gravity and to prevent this, the electrophoretic mobility of the particles have to be higher than the gravity [53]. To have a good quality deposition with large particles either the surface charge must be high or the thickness of the electrical double layer must increase, otherwise using a sedimenting suspension for EPD process will lead to a gradient in deposition, i.e. the film would be thinner on top and thicker at the bottom [53]. The interaction energy between dispersed particles is determined by two mechanisms: electrostatic and van der Waals forces [53]. To avoid particle agglomeration, high electrostatic repulsion is necessary so that particles in the solution can repel each other, which can be obtained with high particle charge [53]. However, when the surface charge is low then there is no force between the particles to prevent them from coming together and agglomerating. Zeta potential analysis was used to determine the surface charge of particles in a solution which can be controlled with pH. The concentrations of solvents and additives plays a key role in preparation of a stable suspension.

There are certain criteria to choose a proper liquid media for EPD; there shouldn't be a chemical reaction with the dispersed particles, but it should be possible to generate charge on the particles surface and finally, fast evaporation is to be avoided to prevent crack formation during drying [41]. In Paper C, EPD films prepared in a solution of ethanol, acetone and triethanolamine (TEA) are presented. Without the addition of TEA, the films were drying very fast due to the evaporation rate of ethanol and acetone. At first 0.05 vol/vol% of TEA is tested in 15 ml solution of

ethanol (25 vol%) and acetone (75 vol%), particle deposition was observed throughout the substrate but the film was drying in few seconds, which caused a lot of cracks on the film (Figure 3.6 (a)). By increasing the amount of TEA in the solution to 0.1 vol/vol%, the drying slowed down and the crack formation was eliminated (Figure 3.6 (b)).

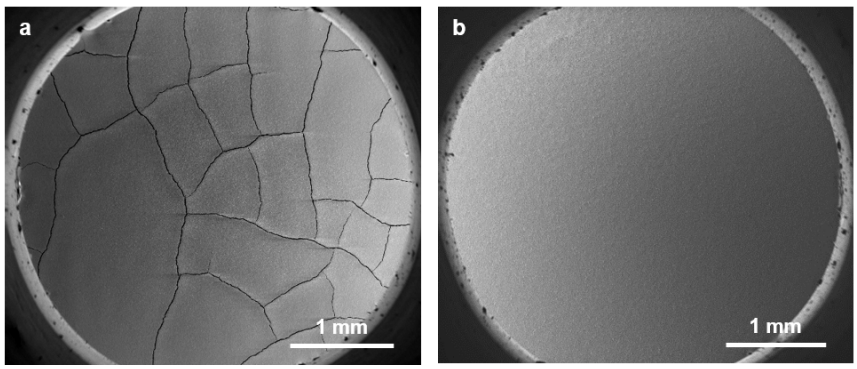

Figure 3.6. SEM micrographs of Bi_2Te_3 films deposited at 50 V and 10 min. In the image a) the crack formation due to the fast drying of deposition is visible and in b), with the adjustment of TEA concentration in the EPD media, the film dried slower and crack formation was eliminated.

The last key interaction to determine the colloidal stability is between the particles and surrounding liquid media, and the parameters that affect this interaction are dielectric constant, conductivity and viscosity of the solvent(s). Electrophoretic mobility of the particles depends on these parameters, and it can be measured with zeta potential analysis. By inserting measured values of mobility into Henry's equation, zeta potential values can be calculated: $\mu=(2\zeta\varepsilon f(\kappa\alpha)/3\eta)$ where μ is the electrophoretic mobility, ζ is the zeta potential, ε is the dielectric constant of the solvent, η is the solvent viscosity, and f($\kappa\alpha$) is Henry's function where κ is the Debye length and α is the particle radius [56, 57]. There are two approximations for f($\kappa\alpha$), one of them is the Smoluchowski approximation where f($\kappa\alpha$)=1.5, this is used in thin double layers and large particles ($\alpha>\kappa$) in aqueous systems [56]. The second one is the Hückel approximation which is generally used for small particles ($\alpha<\kappa$) in non-aqueous systems, since these systems have lower ε, meaning lower ionic concentration and thicker double layer region [56].

Another solvent characteristic that affects the particle mobility is the conductivity of the solvent, which depends on the charged species in the solution (particles and ions), and the polarity of the solvent or of dispersant additives [56]. In the EPD process polar solvents are not generally preferred due to their high ionic concentration and conductivity. For instance,

using aqueous systems in EPD will cause redox reactions on the electrodes' surface, increasing the number of ions in the solution, which hinders the particle mobility and the reduces deposition yield. Thus, for electrophoresis, using solvents with moderate dielectric constant and conductivity is much more advantageous. The last parameter is the viscosity. In Henry's equation we can see the inverse relation between the electrophoretic mobility and viscosity. An ideal EPD media should not have high viscosity, since viscous forces would oppose the movement of charged particles, resulting in low mobility. Deposition yield would be expected to be lower in high viscosity solvents.

It is difficult to determine numerical values for the parameters affecting the EPD process, since every particle and solvent system has different interactions between them. The optimization study is unique for every system and without understanding the effects of these interactions, control of the deposited film quality would not be possible.

Chapter 4

Transport property evaluation

In this Chapter, a short summary of the results from Papers A, B, C, D, and E, regarding the transport property evaluation, are presented and briefly discussed. Measurement setups and estimation process for transport properties are explained. The detailed analysis of the transport property measurements of the TE materials can be found in the dedicated papers.

4.1 Bulk properties (Paper A and B)

Bulk characteristics of $Bi_{2-x}Sb_xTe_3$ (x:0-2) compounds (Paper A) and Bi_2Te_3 particles (Paper B), synthesized via polyol and hydrothermal route, respectively, were studied. As-synthesized particles from each compound were consolidated into a pellet form using SPS method, in a 15 mm diameter die. Pellets of each compound were prepared under the same conditions; 400 °C sintering temperature, 1 min holding time and 50 MPa sintering pressure. The electrical conductivity (σ) and Seebeck coefficient (S) of the pellets were measured simultaneously using an ULVAC-RIKO ZEM3 system. The thermoelectric power factor ($PF=S^2\sigma$), was calculated using S and σ of the each compound. The total thermal conductivity (κ) was estimated with the following equation; $\kappa=C_p\alpha\rho$ where C_p is the specific heat capacity, α is the thermal diffusivity and ρ is the density. C_p was measured with differential scanning calorimetry (DSC), and the α was measured with laser flash analysis system (LFA) by using disk shaped samples with 12.6 mm diameter and 2 mm thickness. ρ is calculated using Archimedes method; $\rho=m/V$ where m is the mass and V is the volume of the pellet. The figure of merit (ZT) was estimated via $ZT=(S^2\ \sigma T)/\kappa$ for each compound.

In Paper A, the transport property measurements were done at the temperature range of 300-523 K for each compound. *S* is the key parameter to determine the transport characteristics of materials (n- or p-type), measurements showed negative *S* for Bi_2Te_3 and $Bi_{1.8}Sb_{0.2}Te_3$ compounds, revealing the n-type properties of the materials (Table 4.1). The positive values of *S* obtained from $Bi_{0.5}Sb_{1.5}Te_3$ and Sb_2Te_3 compounds proven the p-type character of these materials (Table 4.1). The measurements showed that in Bi-rich ternary compounds, the majority of charge carriers are electrons, while in Sb-rich compounds charge carriers are holes. These results indicate that by adjusting the initial ratio of precursor materials in MW-assisted chemical synthesis, it is possible to produce n- and p-type BiSbTe compounds without the necessity of additional stabilizers or post-processing [25].

Table 4.1. The results of transport property measurements done at the temperatures where each compound had their highest ZT values.

Sample	T (K)	κ (W/Km)	*S* (μV/K)	σ (S/cm)
Bi_2Te_3	440	0.87	-159	800
$Bi_{1.8}Sb_{0.2}Te_3$	523	1.05	-129	1047
$Bi_{0.5}Sb_{1.5}Te_3$	523	0.46	+157	275
Sb_2Te_3	523	0.84	+152	942

The lower σ of Bi_2Te_3 compared to Sb_2Te_3 is a result of the intrinsically small band gap (E_g) of Bi_2Te_3, which is around 0.13 eV, and 0.28 eV for Sb_2Te_3 [58, 59]. Doping Bi_2Te_3 with Sb widens E_g, which is a way of optimizing the carrier concentration and introducing strong point defect scattering of phonons. However, due to the differences in micro- and nanostructures of these compounds it is difficult to make direct comparisons of the transport properties. There is an inherent restriction to Sb-doping, since Sb-Te bond has lower polarity compared to the Bi-Te bond, the antisite defects are more severe in Sb_2Te_3 lattice [60]. These intrinsic point defects contribute to the charge carriers, and too many of these defects can lead to a reduction in *S* and an increase in σ and κ_e [60, 61]. On the other hand, an effective way of reducing κ_l is the introduction of more and diverse phonon scattering agents in the crystal, since phonons have a wide spectrum of frequency and wavelength [61]. Above room temperature, intrinsic point defects are very effective scattering centers because the average wavelength of phonons reduces at elevated temperatures [61]. To conclude, doping BiSbTe compounds with either Bi or Sb allows the tuning of transport properties through the changes in E_g, carrier type and concentration, and introduction of defects [9, 60, 61]. The ZT obtained from each compound are promising for TE conversion (Table 4.2).

Table 4.2. A summary of the highest ZT obtained from each compound together with the temperatures and corresponding PF values.

Sample	T (K)	PF ($\mu W/K^2cm$)	ZT
Bi_2Te_3	440	16.52	1.04
$Bi_{1.8}Sb_{0.2}Te_3$	523	15.72	0.87
$Bi_{0.5}Sb_{1.5}Te_3$	523	4.41	0.76
Sb_2Te_3	523	25.37	1.37

In Paper B, the transport property measurements were done at the temperature range of 298-525 K for Bi_2Te_3 particles synthesized via hydrothermal and polyol routes. The measurement results are summarized in Table 4.3 and 4.4. The negative *S* values measured for both samples revealed the n-type transport properties of the materials. In polyol sample, *S* increases with increasing temperature while the hydro sample does not show a strong dependence on temperature. On the other hand, σ of the hydro-sample decreased more drastically with increasing temperature when compared to the polyol-sample. The overall reduction observed in the electrical conductivity with increasing temperature is a typical behaviour of heavily doped semiconductors and metals (Table 4.3). The electronic transport properties are strongly correlated to carrier concentration, microstructure, defects and scattering events. The microstructure of these samples are different from each other, for example the hydro-sample has larger layered structure and the crystallite size is bigger than the polyol-sample [26]. These can be the reasons for the different electronic properties of these two samples with the same composition.

Table 4.3. A summary of transport property measurements done at temperatures 373 and 473 K, on sintered pellets of Bi_2Te_3 particles synthesized via hydrothermal and polyol methods.

Sample	T (K)	κ (W/Km)	*S* (μV/K)	σ (S/cm)
Bi_2Te_3-Hydro	373	0.9	-149	960
	473	1.16	-142	666
Bi_2Te_3-Polyol	373	0.86	-148	929
	473	0.9	-162	758

κ of both samples had a decreasing trend first and then increased with increasing temperature, but in the hydro sample the total increase was more drastic than the polyol-compound. The heat flow is carried by a variety of phonons with different wavelengths and mean free paths (from around 1 nm to 10 μm) creating a need for phonon scattering agents with

different lengths [8]. Therefore, to obtain an efficient phonon scattering throughout the spectrum, nanostructures at different length scales can be used. The two different trends observed in κ of the samples can be a result of the differences in nanostructure of these materials. The slight variation between the calculated ZT is a result of samples displaying a maximum PF and a minimum κ at different temperatures.

Table 4.4. The estimation of power factor (PF) and ZT at 373 and 473 K are presented for both samples.

Sample	T (K)	PF ($\mu W/K^2cm$)	ZT
Bi_2Te_3-Hydro	373	21.31	0.88
	473	13.36	0.54
Bi_2Te_3-Polyol	373	20.36	0.88
	473	19.84	1.03

The development of these time and energy efficient synthetic routes enabled the production of particles with high purity and promising transport properties. Next step was to use these as-made compounds in EPD process to prepare porous TE films.

4.2 EPD film properties (Paper C, D and E)

Electronic transport properties of the nanostructured EPD films of Bi_2Te_3 and Sb_2Te_3 particles were evaluated via the measurement of S and resistance with a two-probe measurement setup shown in Figure 4.1, followed by the calculation of electrical conductivity and power factor of the samples. The film was placed on two separate Cu blocks, where one of them was heated with a Peltier module and the second one was kept at room temperature. S was measured through the integral method, the temperature of the hot side (T_h) of the sample was gradually increased to reach a gradient of 25-30 °C. The generated Seebeck potential between the two ends of the sample was continuously recorded with a source meter. By plotting the potential generated (ΔV) as a function of the temperature gradient (ΔT), a linear distribution was obtained, and S was estimated from the slope of the distribution: $S=\Delta V/\Delta T$. The resistance (R) also measured as a function of temperature, and σ was estimated from R by using the geometrical parameters of the EPD films; $R=l/A\sigma$, where l is the distance between the silver contacts, A is the cross-sectional area, i.e. width multiplied by the thickness of the deposited film. The transport measurements of the EPD films were performed perpendicular to the Cr lines on the substrate to avoid any interruption from the metallic pattern.

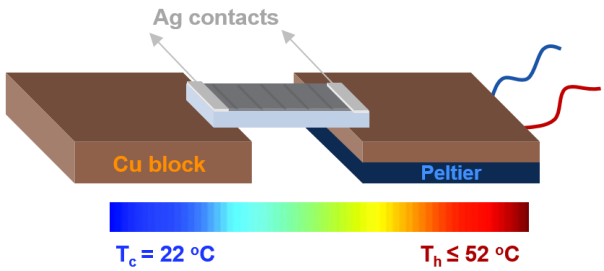

Figure 4.1. A sketch showing the transport property measurement setup where EPD film (light gray) deposited on a glass substrate (light blue) with Cr pattern, placed on two Cu blocks. One side of the film is heated via a Peltier module while the temperature of the other end kept at room temperature. Silver (Ag) contacts placed partially on EPD film and partially on the substrate, and the measurement probes were placed on these Ag contacts.

The new design of glass-based substrate with 10 μm line width and separation distance (Figure 3.2) was tested in several steps to ensure that there is no interference during transport measurements (Figure 4.2). First step was to measure the glass substrate with metallic pattern alone, where an open-circuit behaviour was observed. For the second step, two glass substrates were spin coated; one with 1,6-Hexanedithiol (HDT) and the other with 1-Dodecanethiol (DDT). The electronic transport properties were measured when the coatings were fully dried, and again the results showed open-circuit behaviour. The third step was measuring the EPD films on glass substrate without any molecular linkers. The open-circuit behaviour continued, which was expected from the EPD films due to their porous structure and the high oxide content at the particles' surface. For the fourth step, the EPD films on glass were spin coated with either HDT or DDT, and measured when fully dried. After the addition of these thiol-containing organic molecules, the resistance of the deposited TE films decreased drastically, due to the improved interconnection between particles (Figure 4.3). There has been several studies on using thiol molecules as surface exchange ligands to reduce the oxide layers on nanoparticles and nanowires [62, 63]. Sreeprasad et al. tested different thiol molecules on Te nanowires with TeO_2 layer on the surface, and reported a redox reaction taking place on the particle surface, i.e. the reduction of TeO_2 to Te(0) [63].

In Paper C, the effect of HDT as a molecular linker is tested on various EPD film thicknesses consisting of Bi_2Te_3 particles synthesized via the hydrothermal route. As-made EPD films showed open-circuit behavior before the addition of thiol linkers, and after the spin coating with HDT, the values dropped to the range of 14-17 kΩ, which was attributed to the improved

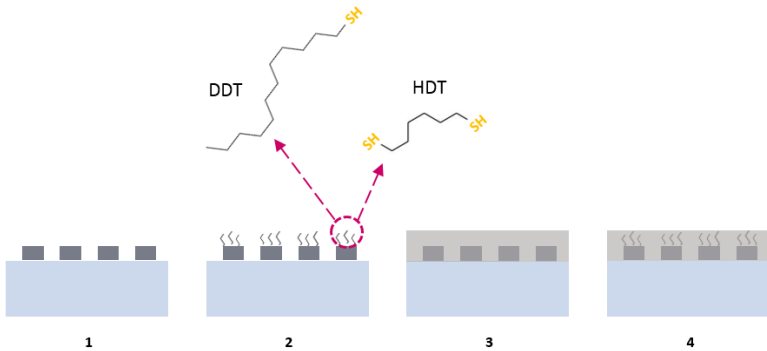

Figure 4.2. Sketch showing the transport measurement steps for the newly designed patterned glass; (1) glass substrate (in blue) with Cr patterned lines (in dark gray); (2) Glass substrate spin coated with HDT or DDT; (3) electrophoretically deposited Bi_2Te_3 or Sb_2Te_3 particles on glass, and (4) HDT or DDT coated EPD film on glass [64].

interconnection between the particles. The sample with thickness of 25-30 μm had a resistance around 11-13 kΩ, and the *S* was in the range of -165 to -180 μV/K which are shown in Figure 4.4(a) and (b), respectively. The resistance linearly drops from 13 to 11.7 kΩ with the increase in T_h to 323 K (50 °C, at ΔT=25 K), revealing the temperature activated transport behavior of semiconductors. In Paper E, Bi_2Te_3 particles synthesized via thermolysis route were used to prepare the TE films, in which HDT and DDT molecules were tested. The resistance of the films which were spin coated with HDT was around 1-2 kΩ, and *S* around -150 μV/K, shown in Figure 4.4(a) and (b). Upon creation of a temperature gradient along the films of Bi_2Te_3 particles, prepared via hydrothermal and thermolysis routes, development of negative Seebeck voltage has been observed, revealing the n-type transport properties as expected from Bi_2Te_3 particles (Figure 4.4(b)). The difference in resistance for these two samples is attributed to the particles' surface chemistry which is a result of different precursors, solvents and synthesis methods used in the material preparation.

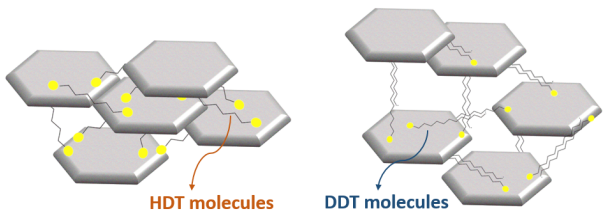

Figure 4.3. The interaction of molecular linkers; HDT and DDT with TE particles.

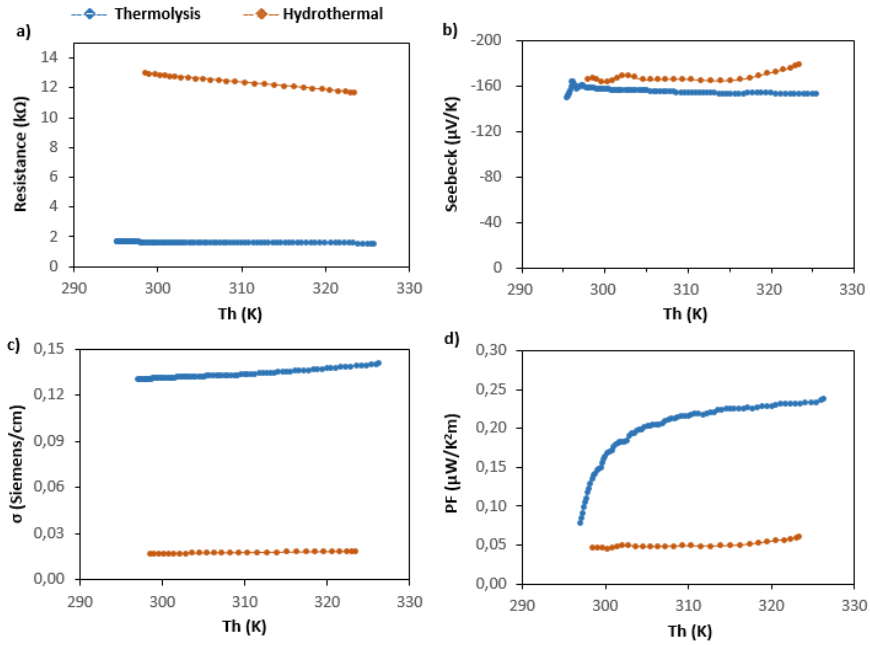

Figure 4.4. The resistance (a), Seebeck coefficient (b), estimated electrical conductivity σ (c), and power factor PF (d) for EPD films of Bi_2Te_3 particles synthesized through hydrothermal and thermolysis routes.

In Paper D, Sb_2Te_3 particles synthesized via thermolysis were used to prepare TE films and the effects of HDT and DDT on electronic transport properties were evaluated (Figure 4.5). The sample coated with HDT was measured at the temperature range of 295-316 K (ΔT=21 K), the sample with DDT measured at higher temperature gradient to observe the trends in ΔT=31 K (295-326 K). The resistance of HDT containing sample decreased from 628 to 607 Ω with increasing temperature. *S* was in the range of 176-185 μV/K which was recorded continuously during heating and cooling, hence, the loop trend is observed for this sample proving the stability of the film (Figure 4.5(b)). The resistance of the DDT coated film decreased from 488 to 475 Ω and *S* decreased from 189 to 168 μV/K. The reducing trend in resistance with increasing temperature observed in both films is a typical behaviour of semiconductors. The positive values of *S* proved the p-type transport character of the Sb_2Te_3 films. The electronic transport properties of the two samples were similar, and the slight differences in *S* can be attributed to the dissimilarities in microstructure.

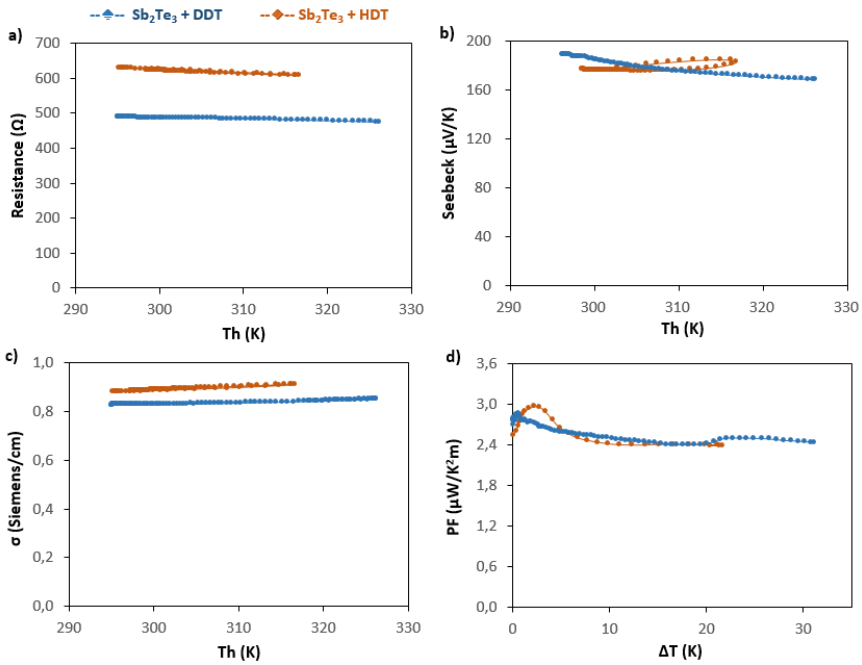

Figure 4.5. The resistance (a), Seebeck coefficient (b), estimated electrical conductivity σ (c), and power factor PF (d) done on EPD films of Sb_2Te_3 particles synthesized through thermolysis route. The films were spin coated with HDT or DDT.

The difficulty in precise estimation of the thickness, porosity, and packing density of these porous EPD films, makes it challenging to calculate the power factor accurately. To have a better understanding of TE performance of the films, the maximum generated power (P) is calculated with the equation $P=V^2/R$, where measured voltage (V) and resistance (R) values are used. An example of this evaluation is presented in Figure 4.6 where Sb_2Te_3 films coated with HDT and DDT were used. The sample with HDT was measured continuously at the temperature range of 295-316 K (ΔT=21 K), the V and R recorded during both heating and cooling (Figure 4.6(a)). The dimensions of this film was 1.3x1.8 cm and thickness was around 25 μm. At ΔT=21 K, estimated power was 23 nW, and at ΔT=20 K it was 19 nW. The sample with DDT was measured continuously at the temperature range of 295-326 K (ΔT=31 K) to observe the trend at higher temperatures, and the V and R recorded only during heating process (Figure 4.6(b)). Film dimensions was 1.4x1.7 cm and thickness was around 30 μm. At ΔT=31 K, estimated power was 58 nW, and at ΔT=20 it was 24 nW. The similarity between the samples can be observed by comparing P at ΔT=20 K.

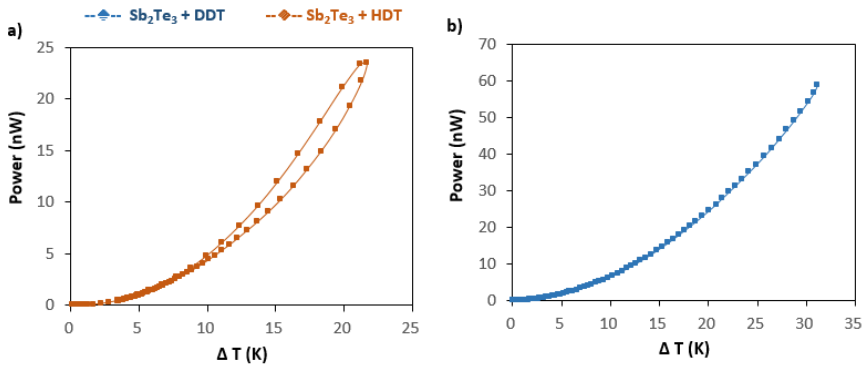

Figure 4.6. The estimation of generated power as a function of temperature difference between the hot and cold side of the Sb_2Te_3 film (a), HDT used as the linker (b), DDT was the linker.

In order to make a TE device n- and p-type films should be connected to form a p-n junction. The power estimations done for the EPD films resulted in power generation in the range of 1-100 nW, and this range can be referred to as ultra-low-power (ULP). With the coming age of the internet of things (IoT), demand for ULP receivers will continue to increase drastically [65]. The IoT can be defined as a network of physical devices embedded with sensors, software and network connectivity, which enables them to collect and share data. These are known as smart devices/objects such as, smart home appliances, and wearables like smart watches. Wireless sensor networks can transmit, receive, and log remote data signals from a broad range of sensors and efficient wireless connectivity is a key requirement for IoT applications [65]. There are wireless data loggers called piconodes which can collect data from various sensors and transmit the data with radio frequency to a gateway connected to internet [65, 66]. Piconodes require ULP consumption to extend the time between battery charging or eliminate the battery usage [66]. These data loggers are compatible with various sensors and can be used in areas such as smart home devices or integrated patient monitoring systems [66]. TE generators perform well for harvesting energy at high temperature differences but for sensors and IoT applications there is need for generators that can operate at low temperature differences [67]. The results of this thesis work showed promising results for building TE modules consisting of electrophoretically deposited Bi_2Te_3 and Sb_2Te_3 films that might be used to harvest energy at low temperature differences and generate ULP for some sensing applications.

Chapter 5

Conclusions and outlook

Smart devices we encounter in almost every aspect of our lives motivate research on improving the efficiency of near-room temperature power generators. Thermoelectrics have some advantages for the applications in this area, such as their lack of noise, moving parts, and no need for regular maintenance. And with the developments in nanotechnology, it is now possible to optimize the synthesis and processing of thermoelectric materials to improve their performances at desired temperature ranges. It is equally important to convert these processes into more environmental-friendly, and time- and energy-efficient routes.

In this thesis, a platform has been developed starting from the synthesis of n- and p-type $Bi_{2-x}Sb_xTe_3$ (x:0-2) compounds, followed by the assembly of as-made particles into pellets and porous films which enabled to study the effects of interfaces/additives on the thermoelectric performance of the films. Three different microwave-assisted synthetic routes have been developed for material synthesis in a matter of few minutes, providing a good control over the particle size, morphology and surface chemistry. As-synthesized particles were consolidated into pellet form via spark plasma sintering, which allowed high compaction densities while keeping the nano-sized structures of the material. The study of bulk characteristics showed consistently low thermal conductivities as a result of nanostructuring of the thermoelectric materials, where the different length scale of these structures acted as phonon scattering centers. The nanostructured thermoelectric materials showed improvements on the figure of merit compared to the literature.

Then, electrophoretic deposition (EPD) was implemented for the preparation of porous nanostructured thermoelectric films. Different formulations of electrolytes, electrodes and substrates were evaluated and optimized to obtain the desired film quality. A newly designed glass-based elec-

trode was used as the substrate for the deposition of thermoelectric particles, which prevented possible interruptions from the metallic substrate during transport property measurements. With this new design of the substrate it was possible to estimate the power factor of the deposited material. As-made thermoelectric films prepared via EPD in a few minutes with various thicknesses showed high resistance values, which was attributed to the high interfacial resistance due to the oxide layers on the particles' surface. After using thiolated organic molecules as additives, the resistance was decreased drastically as a result of improved interconnection between the particles. The promising results obtained from the generated power calculations created the possibility of using EPD films in thermoelectric generators.

The platform developed here enables the investigation of effects of particle size, morphology and molecular linkers on transport properties, which helps to identify the best performing film formulation for specific material compositions. The porous structure of the EPD films also allows the study of ionic liquids and conducting polymers to improve the power factor of the materials.

Summary of papers

Paper A: Facile solution synthesis, processing and characterization of n-and p-type binary and ternary Bi-Sb tellurides

Using microwave-assisted polyol synthesis, large batches of n- and p-type $Bi_{2-x}Sb_xTe_3$ (x:0-2) alloys were synthesized in 2 minutes with over 90% yield. As-made powders exhibit high crystallinity, phase purity, and hexagonal platelet morphology which analyzed via XRPD and SEM. Surface composition and colloidal stability of the particles studied with XPS and zeta potential. Binary and ternary metal chalcogenides consolidated via SPS method and thermoelectric performances of the pellets were evaluated.

Paper B: Minute-made, high-efficiency nanostructured Bi_2Te_3 via high-throughput green solution chemical synthesis

Microwave-assisted hydrothermal and polyol methods used to prepare Bi_2Te_3 nanoparticles. The effects of the synthesis route and solvent selection on physicochemical and transport properties were discussed. As-synthesized particles made with both methods were compared in terms of phase purity, crystallinity and microstructure by using XRPD and SEM. The surface analysis of the particles was done with XPS and zeta potential which showed differences in surface composition due to the precursor and solvent selection of different synthesis routes. The Bi_2Te_3 particles were consolidated via SPS into pallet forms and their thermoelectric performances were evaluated.

Paper C: On the electrophoretic deposition of Bi_2Te_3 nanoparticles through electrolyte optimization and substrate design

Bi2Te3 nanoparticles synthesized using microwave-assisted hydrothermal route, which were used to prepare thermoelectric films via electrophoretic deposition. A special glass-based substrate was designed and fabricated using maskless photolithography, to evaluate the electronic transport properties of the thermoelectric films without the interference of the substrate.

As-made EPD films showed high resistivity, due to the surface oxide layer and capping ligands. After the addition of a dithiol molecular linker, the resistance was significantly reduced. Electrolyte composition was optimized for high mobility of the suspended nanoparticles, and Bi_2Te_3 films were prepared with high deposition rate, reaching 10 μm/min.

Paper D: Electrophoretic assembly and electronic transport properties of rapidly synthesised Sb_2Te_3 nanoparticles

Thermolysis route with microwave-assisted heating was used to prepare Sb_2Te_3 particles. XRPD analysis of as-synthesized particles showed high-phase purity and with rhombohedral crystal structure. Microstructure analysis via SEM showed hexagonal platelet morphology, and some intergrown nanoparticles. Electrophoretic deposition process used to prepare thermoelectric films of Sb_2Te_3 particles, and the evaluation of electronic transport properties of the films showed high resistance. The effects of two type of molecular linkers, single thiol and dithiol, on transport properties were investigated. Changes in surface chemistry with the addition of organic molecules analyzed via XPS.

Paper E: Electrophoretic deposition and characterization of Bi_2Te_3 synthesized through hydrothermal and thermolysis routes

Bi_2Te_3 particles with high phase purity was synthesized using thermolysis and hydrothermal routes. As-made particles used to prepare EPD films under $\leq$3 min deposition time. Microstructure analysis of the thermoelectric films done via SEM, which showed platelet morphology of the particles and porous structure of the films. Surface chemistry of the deposited particles analyzed via XPS after the addition of thiolated organic molecules. Electronic properties of the electrophoretically deposited films were measured and the effects of the synthesis routes and additives were discussed.

Acknowledgements

This thesis work would not be possible without the scientific and emotional support of many people, and I would like to express my deepest gratitude to everyone who was involved.

My supervisor Muhammet S. Toprak, for giving me the opportunity to do my PhD studies in his group. You are an amazing chemist and I have learned a lot from you. Your ideas and guidance were very valuable for this project. Thank your for all the long hours of discussions, the Turkish coffee breaks, and pep talks, they are all appreciated. Jonas Sellberg, for helping me to widen my research area by involving me in different projects. Thank you for your constant support. Muhammet and Jonas, your input was very important for this thesis, thank you for reviewing it.

Hans Hertz, your support and trust in me really made a difference. It was a pleasure working with you. Linda Lundström, I am grateful for your support in these past years, our discussions were very valuable. Peter Unsbo and Carlota Canalias, I am very happy that I had the chance of working with you both. Thank you for keeping your door always open, and being so kind and supportive.

Bejan Hamawandi, for teaching me all the tips and tricks about thermoelectrics, your lab experience really made a difference, I learned a lot from you. Thank you for all your input, your patience and constant support. Adem B. Ergül, your knowledge and experience in nanofabrication changed the course of this project. Thank you for all the long hours of measurements and discussions. All the partners of UncorrelaTEd H2020 FET Open project, it was a pleasure working with you all in these past four years, I have learned a lot from you. Thank you for everything.

AlbaNova Nanofabrication Lab staff, Eric Holmgren and Adrian Iovan, thank you for your patience and help in the clean room. Special thanks goes to Anders Liljeborg for being my KLARA support, and sharing my burden, it was really appreciated.

Petros Papadogiannis for being my rock, laughing, crying, hugging, singing, dancing with me. It would be very difficult to do this without you.

Thomas Frisk for all the interesting discussions, super funny (!) dad jokes, and crash courses in Swedish.

Giovanni and Yuyang for making it fun to work in the lab; Giovanni for singing opera with his beautiful (!) voice, and Yuyang for singing Imagine Dragons with me. It was lovely to work with you guys and thank you for all the emotional support.

Niloo, Jenny, Hanna, Kjell and Klaus, for being amazing office mates. Girls for all the hugs, constant emotional support, office fika breaks, and watching Den stora älgvandringen with me. Kjell and Klaus, I am really happy that I had the opportunity to share an office with you, it was great to hear all the stories, our discussions, and your constant support was very much appreciated.

Thank you to every single member of BIOX for all the BBQs, traditional Turkish breakfasts, after works, Julbords, fika breaks, movie nights and SPA mornings. In BIOX, I had the opportunity to work with amazing scientists and I learned a lot from everyone. I always felt very lucky to be part of this group, and I am grateful to all of you for this memorable experience.

Our great administrators Madeleine Sidoli and Sofia Vigren for their help with everything, and special thanks to Sofia for organizing my defence. The one and only AlbaNova Godsmottagning team: Mats Sundberg, Hugo Svanborg, Kristoffer Spetz, Ove Helin, Markus Ottosson, and Anki Eriksson, you people are just amazing, I really appreciate all the help and support.

My dear friend Sedef, I was lucky to have you by my side in these last years. You were an amazing friend, thank you so much for everything.

Special thanks goes to my very talented sister Doga Batili for designing the cover page of this thesis.

Many people supported me in this journey but none of this would be possible without my parents, sister, uncle, and grandparents. They were the motivation and courage I needed to keep going. Thank you for the constant love, support, and encouragement. This thesis is dedicated to my family.

References

[1] G. Li, S. Shittu, T. M. Diallo, M. Yu, X. Zhao, and J. Ji, "A review of solar photovoltaic-thermoelectric hybrid system for electricity generation", *Energy* **158**, 41 (2018).

[2] D. Maradin, L. Cerović, and A. Šegota, "The efficiency of wind power companies in electricity generation", *Energy Strategy Reviews* **37**, 100708 (2021).

[3] M. I. Yuce and A. Muratoglu, "Hydrokinetic energy conversion systems: A technology status review", *Renewable and Sustainable Energy Reviews* **43**, 72 (2015).

[4] L. Deguenon, D. Yamegueu, A. Gomna, *et al.*, "Overcoming the challenges of integrating variable renewable energy to the grid: A comprehensive review of electrochemical battery storage systems", *Journal of Power Sources* **580**, 233343 (2023).

[5] Y. Kishita, Y. Ohishi, M. Uwasu, M. Kuroda, H. Takeda, and K. Hara, "Evaluating the life cycle CO_2 emissions and costs of thermoelectric generators for passenger automobiles: a scenario analysis", *Journal of Cleaner Production* **126**, 607 (2016).

[6] C. Forman, I. K. Muritala, R. Pardemann, and B. Meyer, "Estimating the global waste heat potential", *Renewable and Sustainable Energy Reviews* **57**, 1568 (2016).

[7] R. Venkatasubramanian, E. Siivola, T. Colpitts, and B. O'quinn, "Thin-film thermoelectric devices with high room-temperature figures of merit", *Nature* **413**, 597 (2001).

[8] G. J. Snyder and E. S. Toberer, "Complex thermoelectric materials", *Nature Materials* **7**, 105 (2008).

[9] I. T. Witting, T. C. Chasapis, F. Ricci, M. Peters, N. A. Heinz, G. Hautier, and G. J. Snyder, "The thermoelectric properties of bismuth telluride", *Advanced Electronic Materials* **5**, 1800904 (2019).

[10] Y. Hosokawa, K. Tomita, and M. Takashiri, "Growth of single-crystalline Bi_2Te_3 hexagonal nanoplates with and without single nanopores during temperature-controlled solvothermal synthesis", *Scientific Reports* **9**, 10790 (2019).

[11] Z. Han, J.-W. Li, F. Jiang, J. Xia, B.-P. Zhang, J.-F. Li, and W. Liu, "Room-temperature thermoelectric materials: Challenges and a new paradigm", *Journal of Materiomics* **8**, 427 (2022).

[12] Z. Hu, Z. Wu, Z. Hu, and Z. Wu, "Growth of Sb_2Te_3 Films by Molecular Beam Epitaxial Method", *Nanostructured Thermoelectric Films* pages 185–219 (2020).

[13] X. Yan, W. Zheng, F. Liu, S. Yang, and Z. Wang, "Thickness effects for thermoelectric property of antimony telluride nanoplatelets via solvothermal method", *Scientific Reports* **6**, 1 (2016).

[14] X. Zhao, X. Ji, Y. Zhang, and B. Lu, "Effect of solvent on the microstructures of nanostructured Bi_2Te_3 prepared by solvothermal synthesis", *Journal of Alloys and Compounds* **368**, 349 (2004).

[15] L. Bulat, V. Osvenskii, and D. Pshenai-Severin, "Influence of grain size distribution on the lattice thermal conductivity of Bi_2Te_3-Sb_2Te_3-based nanostructured materials", *Physics of the Solid State* **55**, 2442 (2013).

[16] B. Poudel, Q. Hao, Y. Ma, Y. Lan, A. Minnich, B. Yu, X. Yan, D. Wang, A. Muto, D. Vashaee, *et al.*, "High-thermoelectric performance of nanostructured bismuth antimony telluride bulk alloys", *Science* **320**, 634 (2008).

[17] Y. Pei, X. Shi, A. LaLonde, H. Wang, L. Chen, and G. J. Snyder, "Convergence of electronic bands for high performance bulk thermoelectrics", *Nature* **473**, 66 (2011).

[18] B. Fu, G. Tang, and Y. Li, "Electron–phonon scattering effect on the lattice thermal conductivity of silicon nanostructures", *Physical Chemistry Chemical Physics* **19**, 28517 (2017).

[19] Y. Zhang, "First-principles Debye–Callaway approach to lattice thermal conductivity", *Journal of Materiomics* **2**, 237 (2016).

[20] G. S. Shendur, M. Abeens, R. Muruganadhan, M. Arivanandhan, M. Premnath, and E. Rajasekaran, "Investigation of nano ceramics added bismuth antimony telluride for energy harvesting applications", *Materials Today: Proceedings* **22**, 879 (2020).

[21] D. Groeneveld, J. D. Koenig, M. Poschmann, H. Groß, W. Bensch, L. Kienle, and J. Wöllenstein, "Time-dependent investigation of a mechanochemical synthesis of bismuth telluride-based materials and their structural and thermoelectric properties", *Royal Society Open Science* **9**, 210714 (2022).

[22] H. Feng, C. Wu, P. Zhang, J. Mi, and M. Dong, "Facile hydrothermal synthesis and formation mechanisms of Bi_2Te_3, Sb_2Te_3 and Bi_2Te_3–Sb_2Te_3 nanowires", *RSC Advances* **5**, 100309 (2015).

[23] Y. Saberi, S. A. Sajjadi, and H. Mansouri, "Comparison of characteristics of Bi_2Te_3 and $Bi_2Te_{2.7}Se_{0.3}$ thermoelectric materials synthesized by hydrothermal process", *Journal of Materials Science: Materials in Electronics* **31**, 18988 (2020).

[24] T. Chiba, H. Yabuki, and M. Takashiri, "High thermoelectric performance of flexible nanocomposite films based on Bi_2Te_3 nanoplates and carbon nanotubes selected using ultracentrifugation", *Scientific Reports* **13**, 3010 (2023).

[25] B. Hamawandi, S. Ballikaya, H. Batili, V. Roosmark, M. Orlovská, A. Yusuf, M. Johnsson, R. Szukiewicz, M. Kuchowicz, and M. S. Toprak, "Facile solution synthesis, processing and characterization of n-and p-type binary and ternary Bi-Sb tellurides", *Applied Sciences* **10**, 1178 (2020).

[26] B. Hamawandi, H. Batili, M. Paul, S. Ballikaya, N. I. Kilic, R. Szukiewicz, M. Kuchowicz, M. Johnsson, and M. S. Toprak, "Minute-made, high-efficiency nanostructured Bi_2Te_3 via high-throughput green solution chemical synthesis", *Nanomaterials* **11**, 2053 (2021).

[27] W. Liu, K. C. Lukas, K. McEnaney, S. Lee, Q. Zhang, C. P. Opeil, G. Chen, and Z. Ren, "Studies on the Bi_2Te_3–Bi_2Se_3–Bi_2S_3 system for mid-temperature thermoelectric energy conversion", *Energy & Environmental Science* **6**, 552 (2013).

[28] W. Wang, Y. Sun, Y. Feng, H. Qin, J. Zhu, F. Guo, W. Cai, and J. Sui, "High thermoelectric performance bismuth telluride prepared by cold pressing and annealing facilitating large scale application", *Materials Today Physics* **21**, 100522 (2021).

[29] C. Kenel, N. R. Geisendorfer, J. Peng, M. A. Grayson, and D. C. Dunand, "Bi_2Te_3 filaments via extrusion and pressureless sintering of Bi_2Te_3-based inks", *MRS Communications* **11**, 818 (2021).

[30] M. Scheele, N. Oeschler, K. Meier, A. Kornowski, C. Klinke, and H. Weller, "Synthesis and thermoelectric characterization of Bi_2Te_3 nanoparticles", *Advanced Functional Materials* **19**, 3476 (2009).

[31] G. Delaizir, G. Bernard-Granger, J. Monnier, R. Grodzki, O. Kim-Hak, P.-D. Szkutnik, M. Soulier, S. Saunier, D. Goeuriot, O. Rouleau, *et al.*, "A comparative study of Spark Plasma Sintering (SPS), Hot Isostatic Pressing (HIP) and microwaves sintering techniques on p-type Bi_2Te_3 thermoelectric properties", *Materials Research Bulletin* **47**, 1954 (2012).

[32] S. Shen, W. Zhu, Y. Deng, H. Zhao, Y. Peng, and C. Wang, "Enhancing thermoelectric properties of Sb_2Te_3 flexible thin film through microstructure control and crystal preferential orientation engineering", *Applied Surface Science* **414**, 197 (2017).

[33] A. Ahmed and S. Han, "Optimizing the structural, electrical and thermoelectric properties of Antimony Telluride thin films deposited on Aluminum Nitride-coated stainless steel foil", *Scientific Reports* **10**, 6978 (2020).

[34] C. Krataithong, K. Srichai, E. Wongrat, and A. Tubtimtae, "Comparative study on the influence of transparent glass substrates for antimony telluride thin films via structural and optical properties", *Journal of Science: Advanced Materials and Devices* **7**, 100449 (2022).

[35] H. Batili, B. Hamawandi, A. B. Ergül, and M. S. Toprak, "On the electrophoretic deposition of Bi_2Te_3 nanoparticles through electrolyte optimization and substrate design", *Colloids and Surfaces A: Physicochemical and Engineering Aspects* **649**, 129537 (2022).

[36] T. Talebi, R. Ghomashchi, P. Talemi, and S. Aminorroaya, "Thermoelectric performance of electrophoretically deposited p-type Bi_2Te_3 film", *Applied Surface Science* **477**, 27 (2019).

[37] S. Seuss and A. R. Boccaccini, "Electrophoretic deposition of biological macromolecules, drugs, and cells", *Biomacromolecules* **14**, 3355 (2013).

[38] R. Sikkema, K. Baker, and I. Zhitomirsky, "Electrophoretic deposition of polymers and proteins for biomedical applications", *Advances in Colloid and Interface Science* **284**, 102272 (2020).

[39] Y. Ma, J. Han, M. Wang, X. Chen, and S. Jia, "Electrophoretic deposition of graphene-based materials: A review of materials and their applications", *Journal of Materiomics* **4**, 108 (2018).

[40] M. Ata, Y. Liu, and I. Zhitomirsky, "A review of new methods of surface chemical modification, dispersion and electrophoretic deposition of metal oxide particles", *RSC Advances* **4**, 22716 (2014).

[41] S. Obregón, G. Amor, and A. Vázquez, "Electrophoretic deposition of photocatalytic materials", *Advances in Colloid and Interface Science* **269**, 236 (2019).

[42] H. Dong, Y.-C. Chen, and C. Feldmann, "Polyol synthesis of nanoparticles: status and options regarding metals, oxides, chalcogenides, and non-metal elements", *Green Chemistry* **17**, 4107 (2015).

[43] S.-H. Feng and G.-H. Li, "Hydrothermal and solvothermal syntheses", in "Modern inorganic synthetic chemistry", pages 73–104, Elsevier (2017).

[44] B. Zhou, Y. Zhao, L. Pu, and J.-J. Zhu, "Microwave-assisted synthesis of nanocrystalline Bi_2Te_3", *Materials Chemistry and Physics* **96**, 192 (2006).

[45] P. A. Mello, J. S. Barin, and R. A. Guarnieri, "Microwave heating", in "Microwave-Assisted Sample Preparation for Trace Element Analysis", pages 59–75, Elsevier (2014).

[46] G. Cravotto, P. Cintas, *et al.*, "1. Microwave chemistry: history, development and legacy", *Microwave Chemistry* pages 1–17 (2017).

[47] G. Akerlof and H. Oshry, "The dielectric constant of water at high temperatures and in equilibrium with its vapor", *Journal of the American Chemical Society* **72**, 2844 (1950).

[48] T. Seward, "Metal complex formation in aqueous solutions at elevated temperatures and pressures", *Physics and Chemistry of the Earth* **13**, 113 (1981).

[49] W.-Y. Wong and Q. Dong, *Functional Nanomaterials: Synthesis, Properties, and Applications*, John Wiley & Sons (2022).

[50] M. Salavati-Niasari, F. Davar, and M. Mazaheri, "Synthesis of Mn_3O_4 nanoparticles by thermal decomposition of a [bis (salicylidiminato) manganese (II)] complex", *Polyhedron* **27**, 3467 (2008).

[51] F. Wang and X. Liu, "1.18 Rare-earth doped upconversion nanophosphors", *Comprehensive Nanoscience and Technology* **1**, 607 (2011).

[52] Y.-W. Zhang, X. Sun, R. Si, L.-P. You, and C.-H. Yan, "Single-crystalline and monodisperse LaF_3 triangular nanoplates from a single-source precursor", *Journal of the American Chemical Society* **127**, 3260 (2005).

[53] P. Sarkar, D. De, T. Uchikochi, and L. Besra, "Electrophoretic deposition (EPD): fundamentals and novel applications in fabrication of advanced ceramic microstructures", in "Electrophoretic Deposition of Nanomaterials", pages 181–215, Springer (2011).

[54] R. N. Basu, C. A. Randall, and M. J. Mayo, "Fabrication of dense zirconia electrolyte films for tubular solid oxide fuel cells by electrophoretic deposition", *Journal of the American Ceramic Society* **84**, 33 (2001).

[55] Y.-C. Wang, I.-C. Leu, and M.-H. Hon, "Kinetics of electrophoretic deposition for nanocrystalline zinc oxide coatings", *Journal of the American Ceramic Society* **87**, 84 (2004).

[56] R. Moreno and B. Ferrari, "Nanoparticles dispersion and the effect of related parameters in the EPD kinetics", in "Electrophoretic deposition of nanomaterials", pages 73–128, Springer (2011).

[57] M. Kaszuba, J. Corbett, F. M. Watson, and A. Jones, "High-concentration zeta potential measurements using light-scattering techniques", *Philosophical Transactions of the Royal Society A: Mathematical, Physical and Engineering Sciences* **368**, 4439 (2010).

[58] G. S. Nolas, J. Sharp, and J. Goldsmid, *Thermoelectrics: basic principles and new materials developments*, volume 45, Springer Series in Materials Science (2001).

[59] R. Sehr and L. Testardi, "The optical properties of p-type Bi_2Te_3 Sb_2Te_3 alloys between 2-15 microns", *Journal of Physics and Chemistry of Solids* **23**, 1219 (1962).

[60] W.-T. Chiu, C.-L. Chen, and Y.-Y. Chen, "A strategy to optimize the thermoelectric performance in a spark plasma sintering process", *Scientific Reports* **6**, 23143 (2016).

[61] T. Zhu, L. Hu, X. Zhao, and J. He, "New insights into intrinsic point defects in V2VI3 thermoelectric materials", *Advanced Science* **3**, 1600004 (2016).

[62] E. J. D. Klem, H. Shukla, S. Hinds, D. D. MacNeil, L. Levina, and E. H. Sargent, "Impact of dithiol treatment and air annealing on the conductivity, mobility, and hole density in PbS colloidal quantum dot solids", *Applied Physics Letters* **92**, 212105 (2008).

[63] T. Sreeprasad, A. K. Samal, and T. Pradeep, "Bending and shell formation of tellurium nanowires induced by thiols", *Chemistry of Materials* **21**, 4527 (2009).

[64] H. Batili, B. Hamawandi, P. Parsa, A. B. Ergül, and M. S. Toprak, "Electrophoretic Assembly and Electronic Transport Properties of Rapidly Synthesized Sb_2Te_3 Nanoparticles", *Applied Surface Science* **637**, 157930 (2023).

[65] D. D. Wentzloff, A. Alghaihab, and J. Im, "Ultra-low power receivers for IoT applications: A review", in "2020 IEEE Custom Integrated Circuits Conference (CICC)", pages 1–8, IEEE (2020).

[66] V. Mangal and P. R. Kinget, "28.1 A 0.42 nW 434MHz-79.1 dBm wake-up receiver with a time-domain integrator", in "2019 IEEE International Solid-State Circuits Conference-(ISSCC)", pages 438–440, IEEE (2019).

[67] M. Al Musleh, E. V. Topriska, D. Jenkins, and E. Owens, "Thermoelectric generator characterization at extra-low-temperature difference for building applications in extreme hot climates: Experimental and numerical study", *Energy and Buildings* **225**, 110285 (2020).